Cost Effective Soft Material Conductivity, Temperature, and Depth (CTD) Sensors

Final Report

Award No. N00014-19-1-2673

Submitted by,
The Johns Hopkins University Applied Physics Laboratory
11100 Johns Hopkins Road, Laurel, MD 20723-6099

To: Dr. Reginald Beach
Office of Naval Research

From: Dr. Morgan Trexler, Program Manager
Dr. Leslie Hamilton, Project Manager, Assistant Program Manager
Science of Extreme and Multifunctional Materials

Reporting Period: September 1, 2019 to April 30, 2023

Reference Number: REDD-2023-320

REPORT DOCUMENTATION PAGE

1. REPORT DATE	2. REPORT TYPE	3. DATES COVERED START DATE	3. DATES COVERED END DATE
20230602	Final Report	9/1/2019	4/30/2023

4. TITLE AND SUBTITLE
Cost Effective Soft Material Conductivity, Temperature, and Depth (CTD) Sensors

5a. CONTRACT NUMBER	5b. GRANT NUMBER	5c. PROGRAM ELEMENT NUMBER
N00014-19-1-2673	Grant12773040	ONR
5d. PROJECT NUMBER	**5e. TASK NUMBER**	**5f. WORK UNIT NUMBER**
	FGE08	

6. AUTHOR(S)
Hamilton, Leslie H., Dr.

7. PERFORMING ORGANIZATION NAME(S) AND ADDRESS(ES)	8. PERFORMING ORGANIZATION REPORT NUMBER
The Johns Hopkins University 3400 N. Charles St. Baltimore, MD 21218	REDD-2023-320

9. SPONSORING/MONITORING AGENCY NAME(S) AND ADDRESS(ES)	10. SPONSOR/MONITOR'S ACRONYM(S)	11. SPONSOR/MONITOR'S REPORT NUMBER(S)
Office of Naval Research 875 N. Randolph St. Suite 1425 Arlington, VA 22203	ONR	

12. DISTRIBUTION/AVAILABILITY STATEMENT
Approved for Public Release; Distribution is Unlimited

13. SUPPLEMENTARY NOTES

14. ABSTRACT
Conductivity (salinity), Temperature, and Depth (pressure) (CTD) are the fundamental scalars that oceanographers require to explain variability of oceanic processes. Today, a number of compact self-logging CTD systems (such as RBRbrevio3 and Seabird SBE 49) exist that accurately measure the seawater properties. These CTD sensors are configured such that transducers are mounted onto the outside of a waterproof chamber with various water-resistant seals. The electronics and batteries are located inside the waterproof chamber that is able to withstand large hydrostatic pressures. To withstand different magnitudes of ocean pressure, different materials are chosen for the chamber housing material, including titanium alloys for deep ocean deployment and poly(vinyl chloride) material for shallow waters. Systems are designed around the rigid cylindrical pressure chambers, which cannot easily be modified into alternative forms. Currently, CTD systems are relatively expensive, where expense is associated with sensor accuracy, resolution, duration, storage, and waterproof chamber. Furthermore, traditional CTD sensors are prone to marine biofouling, which greatly reduces the in situ operational use .

The goal of this project was to develop a low-cost, soft-material sensor platform for oceanic salinity, temperature, and pressure (CTD) sensing. Throughout this project, we executed against the following objectives (1): Novel sensor development, (2): Novel soft materials with antifouling properties, (3): System level design and prototype development.

PREVIOUS EDITION IS OBSOLETE.

STANDARD FORM 298 (REV. 5/2020)
Prescribed by ANSI Std. Z39.18

15. SUBJECT TERMS
Grants, CTD Sensors, Novel Sensors, Novel Materials, Prototype Development

16. SECURITY CLASSIFICATION OF:			17. LIMITATION OF ABSTRACT	18. NUMBER OF PAGES
a. REPORT	b. ABSTRACT	C. THIS PAGE	UU	25
U	U	UNCLASSIFIED		

19a. NAME OF RESPONSIBLE PERSON	19b. PHONE NUMBER *(Include area code)*
Dr. Leslie H. Hamilton	240-228-1091

PREVIOUS EDITION IS OBSOLETE.

STANDARD FORM 298 (REV. 5/2020)
Prescribed by ANSI Std. Z39.18

I. Project Overview

Conductivity (salinity), Temperature, and Depth (pressure) (CTD) are the fundamental scalars that oceanographers require to explain variability of oceanic processes. Today, a number of compact self-logging CTD systems (such as RBRbrevio3 and Seabird SBE 49) exist that accurately measure the seawater properties. These CTD sensors are configured such that transducers are mounted onto the outside of a waterproof chamber with various water-resistant seals. The electronics and batteries are located inside the waterproof chamber that is able to withstand large hydrostatic pressures. To withstand different magnitudes of ocean pressure, different materials are chosen for the chamber housing material, including titanium alloys for deep ocean deployment and poly(vinyl chloride) material for shallow waters. Systems are designed around the rigid cylindrical pressure chambers, which cannot easily be modified into alternative forms. Currently, CTD systems are relatively expensive, where expense is associated with sensor accuracy, resolution, duration, storage, and waterproof chamber. Furthermore, traditional CTD sensors are prone to marine biofouling, which greatly reduces the *in situ* operational use .

The goal of this project was to develop a low-cost, soft-material sensor platform for oceanic salinity, temperature, and pressure (CTD) sensing, see Figure 1. To this end, we executed against the following objectives:

- *Objective (1): Novel sensor development*. We have developed two novel pressure sensing platforms: (1): Thermoplastic urethane (TPU) and carbon nanotube (CNT) based nano-composites and (2): Carbon dioxide laser induced graphene (LIG) on Kapton substrate.
- *Objective (2)*: *Novel soft materials with antifouling properties*. We have developed and characterized novel antifouling coatings designed specifically to interface with organic materials.
- *Objective (3)*: *System level design:* We demonstrated electronics integration with a Iridium Satellite Constellation communication and a commercially available pressure sensor.

Our multidisciplinary team, consisting of materials scientists, electrical engineers and oceanographers at Johns Hopkins University Applied Physics Laboratory (APL), the Johns Hopkins University (JHU), BlackSky Aerospace LLC, and the Naval Postgraduate School (NPS), has made substantial progress towards the objectives above, discussed herein.

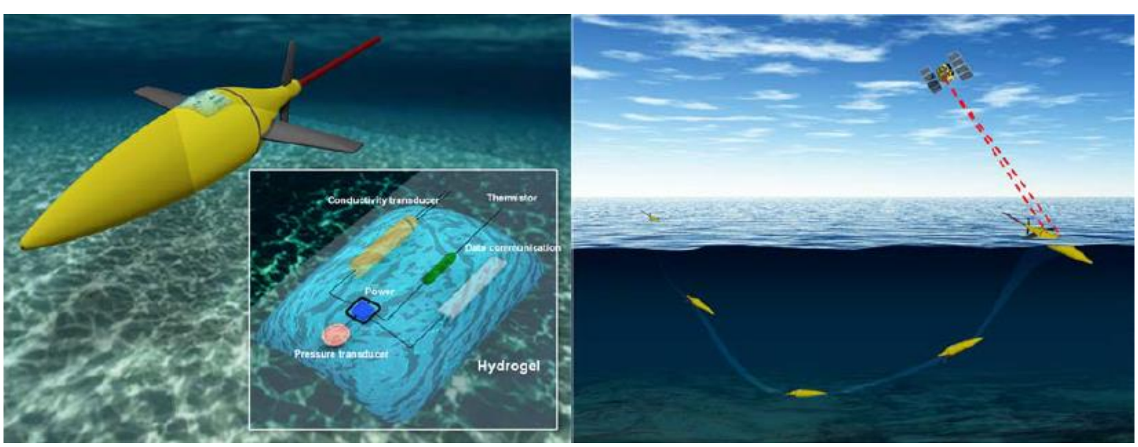

Figure 1: Conceptual sketch showing Cost Effective Soft Material CTD attached onto curved glider surface (left) and a schematic showing the working principle of the sensor coupled with an ocean glider. Not drawn to scale.

II. Technical Accomplishments

The goal of this project was to develop a low-cost, soft-material sensor platform for oceanic salinity, temperature, and pressure (CTD) sensing. To this end, we executed against the following objectives: *(1): Novel sensor development*, *(2)*: *Novel soft materials with antifouling properties*, *(3)*: *System level design*: including electronics and communication capabilities, packaged in a marine-grade soft material.

A. Objective 1: Novel sensing development

Summary: Small, low power, and inexpensive deep ocean pressure sensors are of interest for a myriad of applications from maritime security to environmental monitoring. The team developed and characterized two novel pressure sensing platforms: (1) Thermoplastic urethane (TPU) and carbon nanotube (CNT) based nano-composites and (2) Carbon dioxide laser induced graphene (LIG) on Kapton substrate. While both sensors are promising, neither were ready for integration into a full prototype. In an effort to demonstrate a functional prototype, we also investigated a third platform: (3) Commercially available piezoresistive sensors.

Platform (1): Thermoplastic Urethane (TPU) and Carbon Nanotube (CNT) Based Nano-composites

Our goal was to create a low-cost, novel nano-composite pressure sensor able to withstand high pressures (up to 10 MPa or roughly 1000 m ocean depth). To achieve this objective, we established methods to create composites, we formed the composites into final sensor geometry, we explored the effects of carbon nanotube/graphene loading and matrix stiffness on response range and sensitivity, and fabricated and characterized the resultant sensors. Detailed protocols and results are discussed in our publication[1].

To fabricate composite materials, multiwall CNTs were mixed with a solvent and placed in an ultrasonic bath. TPU was added, and the mixture was returned to an ultrasonic bath. The nanocomposite was optimized for CNT loading, solvent type, and matrix stiffness. The TPU/CNT solution was added to stirring water to drive off and dilute the solvent, and allow the CNT/TPU mixture to solidify. The water in the bath was replaced until all solvent was removed and the materials were dried in a vacuum.

We leveraged an in-house microcompounder to make thermoplastic polyurethane TPU/CNT piezoelectric nanocomposites. Optimized synthesis procedures were developed with a focus on robustness, repeatability, and uniformity. Once synthesized and dried, the TPU/CNT material was formed into the desired shape via injection molding. This process was shown to produce uniform samples. Photographs of injection-molded pieces, both plain TPU and TPU/CNT nanocomposites, are shown in Figure 2. Representative scanning electron microscopy (SEM) images of sensor cross section were collected to examine internal composite morphology, shown in Figure 3. Injection molding led to no obvious voids or pitting. In this case the surface is not coated, but appears conductive, confirming uniform distribution of CNTs. (Right) Conductive and non-conductive areas are apparent, illustrating areas of high CNT concentration and overall uniform distribution.

[1] https://doi.org/10.3390/s22145268

Figure 2: (Left) Injection molded sample made of plain thermoplastic urethane (TPU) (Estane 58881, left). (Right) Injection molded sample of composite material (TPU/CNT ~4wt%).

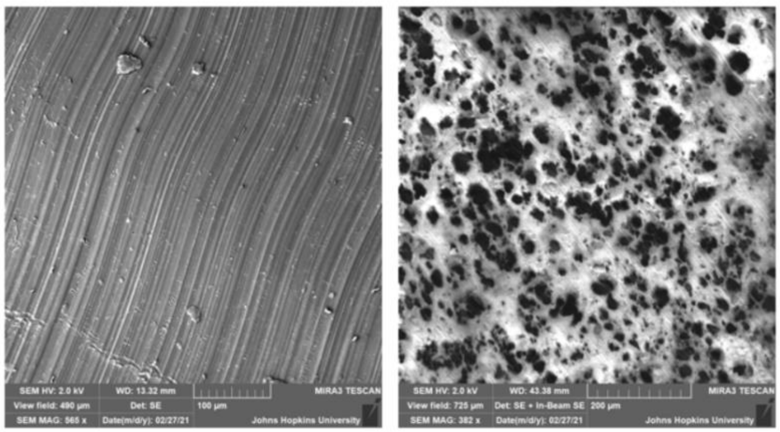

Figure 3: Representative SEM images of sensor cross section. (Left) Injection molding led to no obvious voids or pitting. In this case the surface is not coated, but appears conductive, confirming uniform distribution of CNTs. (Right) Conductive and non-conductive areas are apparent, illustrating areas of high CNT concentration and overall uniform distribution.

JHU conducted a design of experiments (DoE) to characterize the influence of several composite synthesis parameters (CNT loading, solvent type, TPU moduli) on the observed sensor response. Sensor recipes were down-selected to recipes that had an initial resistance < 1 MΩ to ensure the sensing electronics had sufficient sensitivity. APL characterized the piezoresistive performance via uniaxial compression testing (Instron 6800 series 300 kN load frame). To approximate hydrostatic test performance in this configuration, we fabricated a non-conductive Teflon die press to constrain the sensor geometry. TPU/CNT samples and the test setup are shown in Figure 4.

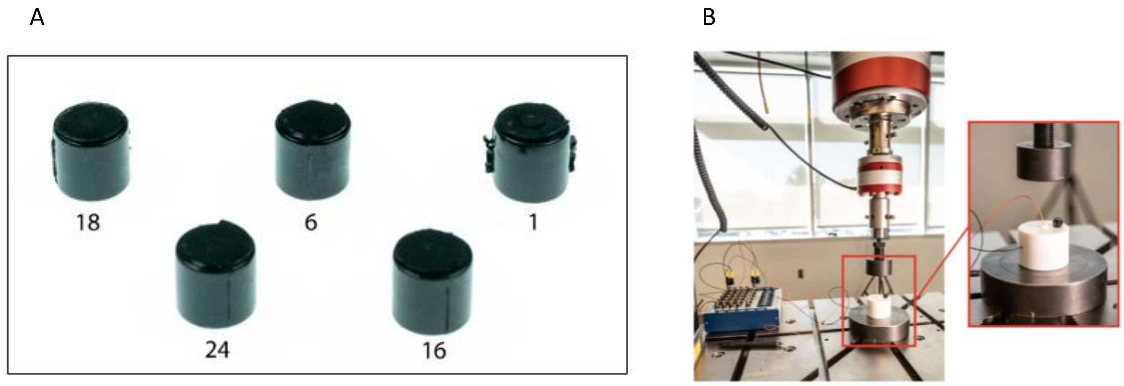

Figure 4: TPU/CNT sensors included in Instron compression testing. Sensors are approximately 10 mm in height and diameter.

Samples were placed within the cavity of the die, and a Teflon plunger was used to compress the samples to 1500 psi (equivalent to approximately 1 km of ocean depth) with the load frame. A small hole within the body of the die and the plunger allowed wires to contact both the top and bottom surfaces of the sensor, and the resistance was recorded with a voltage divider connected to a multifunction I/O device (National Instruments). Voltage values for resistance, load, and displacement were recorded and resistance was calculated based on a voltage divider equation. Example results are shown in Figure 5. Though all sensors showed a rapid resistance decrease with applied pressure, and a subsequent resistance increase when the load was released, Sample 1 showed the largest change in resistance (~1.4 kΩ), Figure 5(A). To test the repeatability of the response, Sample 1 was subjected to three subsequent load profiles, and similar resistance drops were seen for each Figure 5(B).

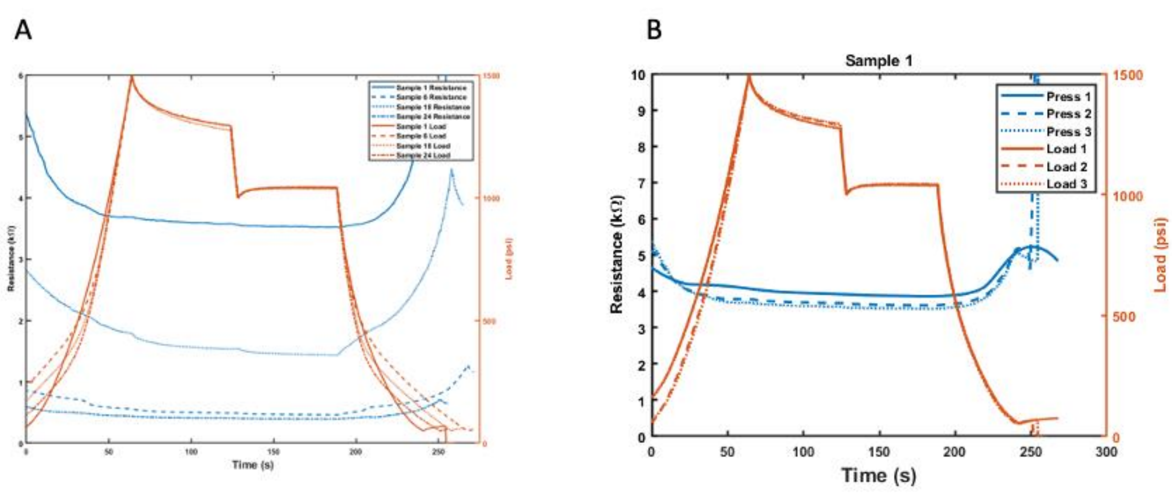

Figure 5: (A) Resistance (blue) and load (orange) profiles of four TPU/CNT composite sensors (samples 1, 6, 18, and 24). Load was increased at a constant displacement (0.01 inch/min) up to 1500 psi, held for one minute, unloaded to 1000 psi, held for another minute, and then unloaded completely. (B) Resistance profiles of the best performing TPU/CNT composite sensor (sensor 1) in three successive loads. Good agreement between runs is seen.

To evaluate higher pressure profiles, one sample (Sample 16) was subjected to three loads of increasing pressure: *(1)* 1500 psi (~1030 m), *(2)* 2500 psi (~1720 m), and *(3)* 4000 psi (~2750 m). The sensor recovered fully each time, though the Teflon mold was permanently deformed in the final press. Results are shown in Figure 6.

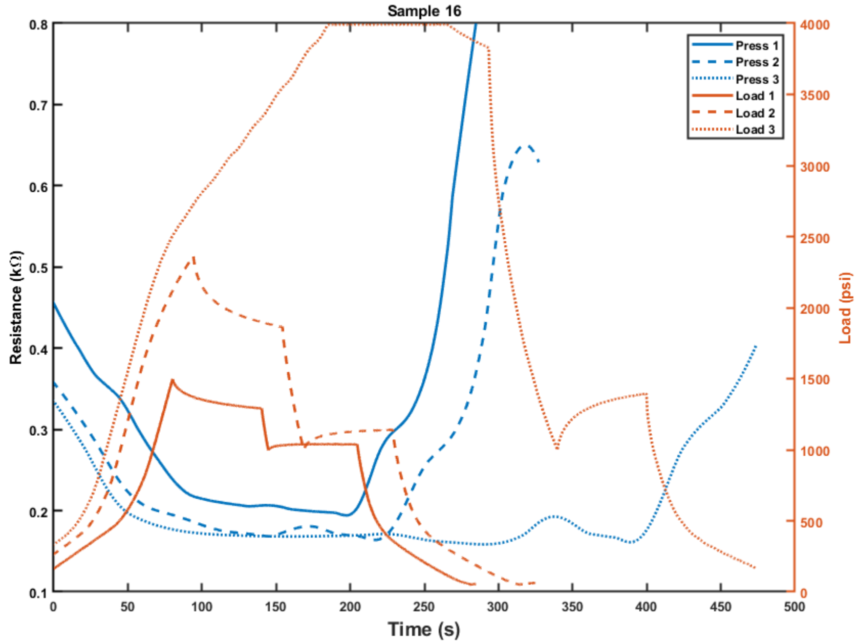

Figure 6: Sensor resistance (blue) and Instron load profiles (orange) for TPU/CNT sensor 16. Loads at constant displacement up to 1500 psi, 2500 psi, and 4000 psi.

To characterize sensors under true hydrostatic pressure, we attempted hydrostatic tank testing. Electrically connected and encapsulated TPU/CNT sensors prepared specifically for tank testing are shown in Figure 7. We used conductive silver epoxy and copper tape to adhere two wires to either side of the sensor. Sensors were encapsulated with silicone (DOW Sylgard 184), allowing for electrical isolation of the sensors from water. We first assessed thermal performance of encapsulated sensors over a relevant ocean temperature range, and then attempted to characterize the performance with hydrostatic tank testing.

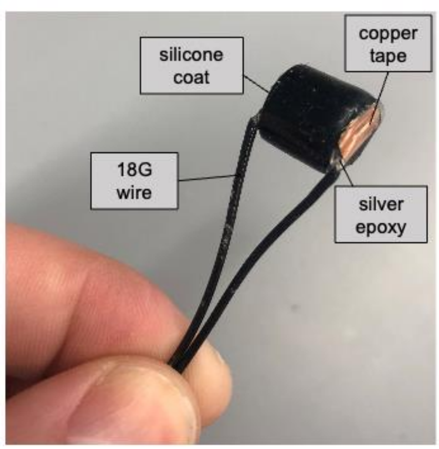

Figure 7: Electrically connected and encapsulated TPU/CNT sensors prepared for hydrostatic tank testing.

Thermal Testing

To characterize thermal response, a 250 mL jacketed beaker was filled with tap water, and the sensor placed inside. A chiller was connected to the inlet and outlet of the jacket allowing coolant to chill the beaker from room temperature to 1°C. The temperature of the tap water was recorded. The resistance of the sensor was measured using a voltage divider connected to a multifunction I/O device (National Instruments). Voltage values for resistance, load, and displacement were recorded using DAQ Express software (National Instruments), and resistance was calculated based on a voltage divider equation with 5V DC power input and a 10 kΩ reference resistor. Between samples, the tap water was refreshed, and coolant allowed to return to room temperature. The performance of the four tested samples is shown in Figure 8. For all sensors, the resistance decreases with increasing temperature, consistent with the negative temperature coefficient of carbon. For all samples, the change in resistance is approximately 0.1 kΩ between 1°C and 25°C.

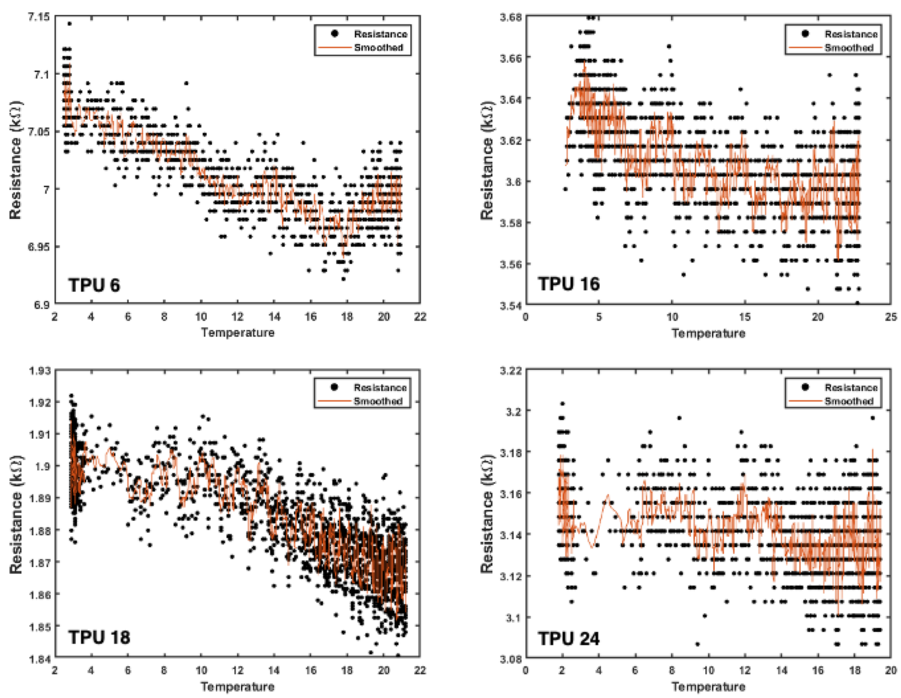

Figure 8: Characterization of resistance as a function of temperature for four CNT/TPU composite pressure sensors.

Hydrostatic Tank Testing

We performed hydrostatic testing using a 76-gallon tank filled with freshwater (Figure 9(A)). The sensor board included the four best performing TPU recipes during Instron testing (Inset, sensors 6, 16, 18, and 24 are shown), which corresponds to different carbon loadings and fabrication parameters. Each sensor's bare wire leads were soldered on a printed circuit board (PCB) to the 5V DC power source via a SubConn six pin connector that mated with the built in connector on the underside of the tank lid. The sensors shared a common ground, allowing for simultaneous data collection of all four sensors at one second intervals. The board was coated in 10 wt% silicone (DOW Sylgard 184) to electrically isolate before testing. The board was attached to the basket and the sensors were allowed to float freely in the water. A pump system pressurized the tank up to 1500 psi at intervals shown in Figure 9(B). Sensors were pressurized to 50 psi, allowed to equilibrate for three minutes, pressurized to 1000 psi, equilibrated for three minutes, pressurized to 1500 psi, equilibrated for three minutes, depressurized to 1000 psi for three minutes, and finally depressurized to 50 psi for three minutes. The load and unload cycle was repeated two more times to assess recovery of the sensors. Unfortunately, the noise of the measurement setup and sensors was greater than the change in resistance. This could be from a number of factors including turbulence within the tank, Joule heating of the sensors over time, temperature changes within the tank, or electrical connections. Based on these results, the characterization of TPU/CNT sensors was paused to focus on our second sensor platform, the LIG pressure sensors.

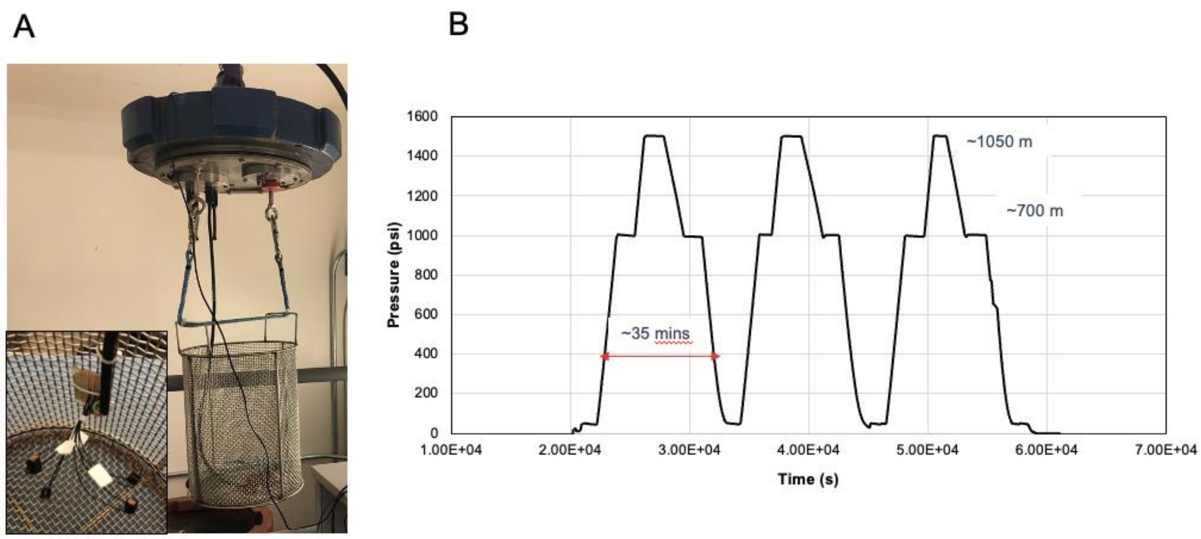

Figure 9: (A) Hydrostatic tank used to assess sensor performance for TPU/CNT sensors. (B) Pressure profile. The tank was pressurized up to 1500 psi at intervals shown above. Equivalent depths of 700 m and 1050 m are shown.

Platform (2): Laser Induced Graphene (LIG) Pressure Sensors

Summary: We optimized fabrication of LIG sensors and explored the practicality of LIG integration into fieldable CTD sensors. While initially promising, we found that the repeatability of sensor fabrication on pressure response, and the thermal dependence of measurements, present challenges for widespread deployment.

Background: LIG sensors have also been previously proposed as deep ocean CTD sensors due to their low cost, rapid fabrication, and tolerance to the extreme pressures and cold temperatures of the ocean. Recent work tested LIG sensors in a compression chamber, simulating depths up to two kilometers, with sensitivities in the relative change in resistance of 2×10^{-5} kPa^{-1} from 0 to ~6 MPa and 0.2×10^{-5} kPa^{-1} from ~6 to ~12 MPa. This demonstrated the feasibility of LIG pressure sensors as deep ocean pressure sensors. However, LIG films are notoriously tricky to fabricate repeatedly, as the morphology of graphene formed depends on the laser power, speed, beam size, focal height, atmosphere, substrate, and more. It is also very difficult to form good electrical connections with the LIG films, as the high surface area makes them near impossible to wet with solder without surface modification. We specifically explored the impact of laser fluence on LIG surface morphology and resistivity, the repeatability of fabrication and response with uniaxial compression testing, and the impact of thermal response with LIG sensors before and after conformal coatings.

LIG Fabrication

Laser induced graphene (LIG) structures were printed on polyimide films with an adhesive backing layer using a commercial laser cutter (Epilog Fusion M2). Initially, we determined the laser parameters that formed good resistive LIG films with our laser system setup. We first found the minimum linewidth resolution (0.5 mm) and spacing (0.3 mm) that repeatedly formed LIG structures. Next, a design of experiment (DoE) approach was used to both find printable recipes and determine the most impactful print parameters on LIG resistivity. From this analysis, it was found that laser speed and power are the most important variables for print quality and linewidth and power are most important influential variables for feature resistance. Results are shown in Figure 10.

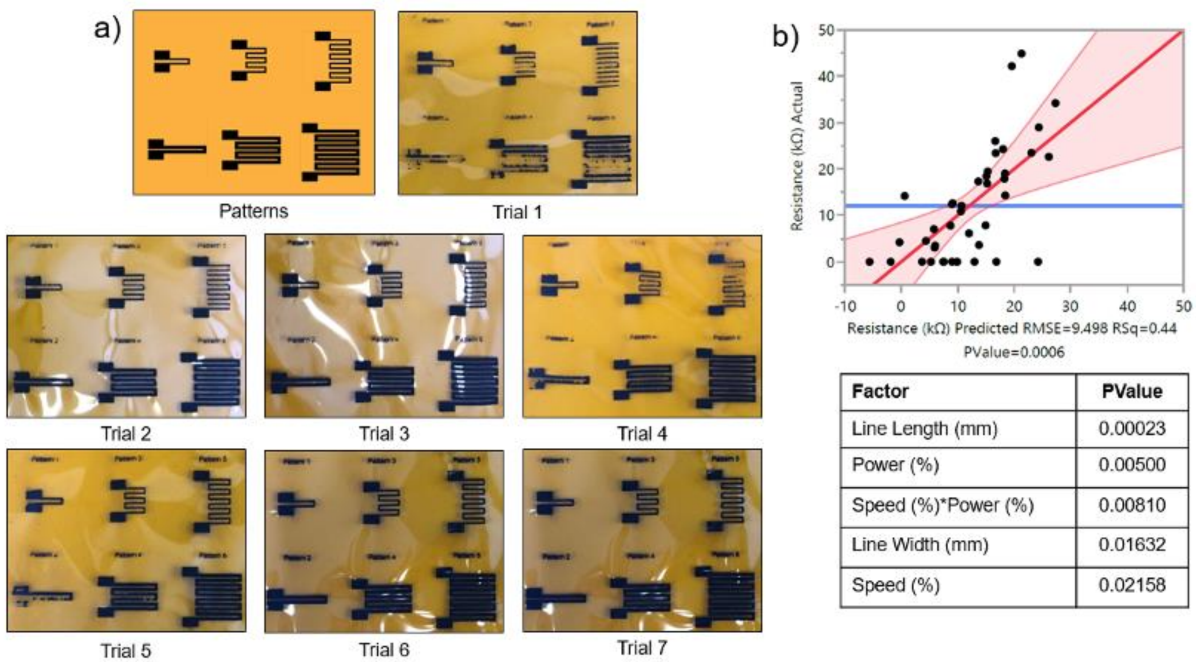

Factor	PValue
Line Length (mm)	0.00023
Power (%)	0.00500
Speed (%)*Power (%)	0.00810
Line Width (mm)	0.01632
Speed (%)	0.02158

Figure 10: DoE analysis for optimizing print quality and resistance (a) print trials, (b) expected vs. predicted values with significant factors.

Four LIG recipes were down-selected for further testing, shown in

Table 1. The laser fluences (H), or energy per area (J/cm^2), for each recipe were also calculated using the following relationship: H = (P/(S x d x PPI)). Speed (S) and power (P) are represented as percentages of the maximum for the laser cutter, d refers to the laser beam diameter (0.076 – 0.127 mm), and PPI refers to the pulse density of the laser (pulses per inch). The laser fluences are estimated values, because though

power scales linearly with percentage, speed does not and is affected by things such as the position of the print on the print bead (i.e., acceleration).

Table 1. LIG recipes down-selected for testing.

Name	Power (%)	Speed (%)	Laser Fluence (J/cm^2)
P45S65	45	65	6.5
P50S65	50	65	7.2
P55S70	55	70	7.4
P60S55	60	55	10.2

To characterize the repeatability of fabrication, at the beginning of each fabrication run, we printed a test swatch with varying line lengths and widths (Figure 11(A)). We then calculated resistivity for each recipe, and compared to previous sensors (Figure 11(B)). To assess the effect of laser recipe on morphology, we collected SEM images of the sensors (Figure 11(C)). In general, as laser fluence increases, resistivity decreases. However, we found that variation in LIG fabrication between batches is greater than variation between tested LIG recipes (speeds and powers). This can be seen in the overlapping error bars as laser fluence increases (Figure 11(B)). The higher average resistivity values of the 7.4 J/cm^2 recipe compared to the 7.2 J/cm^2 recipe is most likely due to the non-linearity of the speed percentage. While the laser fluence values were calculated as if this was a linear value in accordance with manufacturer recommendations, the actual scaling is only approximately linear. SEM images show that as laser fluence increases, larger and more frequent pores form, and cross-sectional images show the formation of fibrous structures on the LIG surface, consistent with literature. Overall, results indicate that our current laser cutting system is not precise enough to produce replicate recipes, and each sensor will have to be individually characterized before deployment. Moving forward, no distinction is made between LIG recipe.

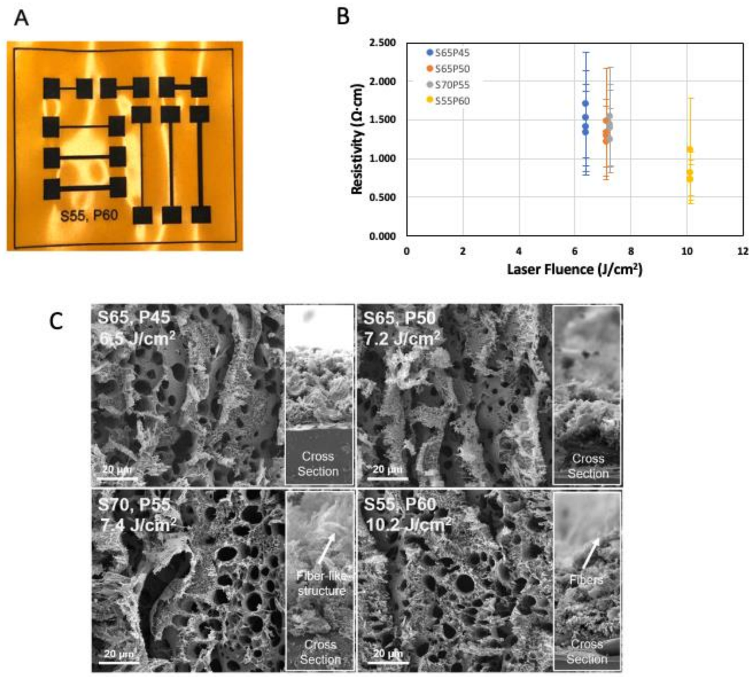

Figure 11: (A) Sample test print to assess sensor/print variability. (B) Resistivity as a function of laser fluence, and morphology as a function of laser fluence. (C) Representative SEM images of LIG produced with varying laser fluence.

Uniaxial Compression Testing

To determine the piezoresistive performance, LIG prints were connected to stainless steel wire leads using silver epoxy and copper tape. For this test, the sensors were sandwiched between two 0.5” thick steel blocks to protect the load cell during compression with thin Kapton sheets (~200 µm). A smaller piece of Kapton tape secured the lead wires in place, but the LIG surface remained uncoated. To prevent shorting with the steel blocks, a piece of Kapton tape coated the underside of the top steel block. Experimental setup and select results are shown in Figure 12. Load cycles were repeated two more times without removing the sample from the test fixture. The results for each sensor recipe show that the influence of re-leveling the bed height is more significant than changing the recipes (speed and power settings) between prints. The difference between samples was often greater than the change in resistance with pressure and the change between recipes. This again indicates that our current laser cutting system is not precise enough to produce replicate recipes, and each sensor would have to be individually characterized before deployment.

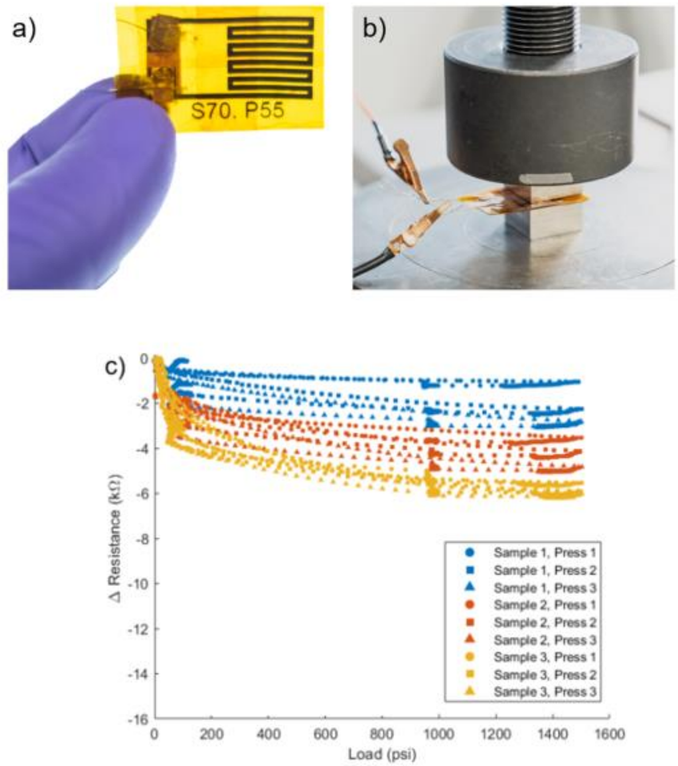

Figure 12: Instron compression testing of LIG sensors during repeated presses. LIG sensors were assembled (a) with steel wire, copper tape, and silver epoxy and loaded under the compression fixture (b) experimental setup of sensor sandwiched between two steel blocks, and (c) change in resistance over the pressure cycle (0.01"/s displacement to 1500 psi, one-minute hold, 0.01"/s displacement to 1000 psi, hold one minute, displacement to ~50 psi). Colors indicate same samples, and marker shapes indicate subsequent presses.

Thermal Testing

Best performing LIG sensors were subjected to thermal testing to characterize the influence of temperature on resistive response. The first measurement setup was the same as mentioned previously for TPU/CNT sensors. In addition, four different electrical isolation strategies were used to electrically isolate the samples from water. This test was to identify the best methodologies for encapsulation including 1) thick (>5 mm) 10 wt% silicone layers, 2) single dip coated layer of 5 wt% silicone, 3) double dip coated layer of 5 wt % silicone, and 4) ultrathin (~25 um) parylene-c layer. A comparison of the resistance versus temperature plots is included in Figure 13. From here you can see that all sensors show a decrease in resistance with increasing temperature, consistent with the TPU/CNT sensors and graphene's negative temperature coefficient of resistance. An ideal sensor would change its resistance only slightly with temperature, so the conformal coatings are ranked from two layers of 5 wt% silicone ($\Delta R \approx 0.2$ kΩ) as the best performer with an ultrathin layer of parylene-c ($\Delta R \approx 1.2$ kΩ) as the worst. This latter value is on par with some of the measured resistance changes over the 1500 psi pressure range during Instron testing, underlining the importance of temperature compensation for resistance measurements in the field.

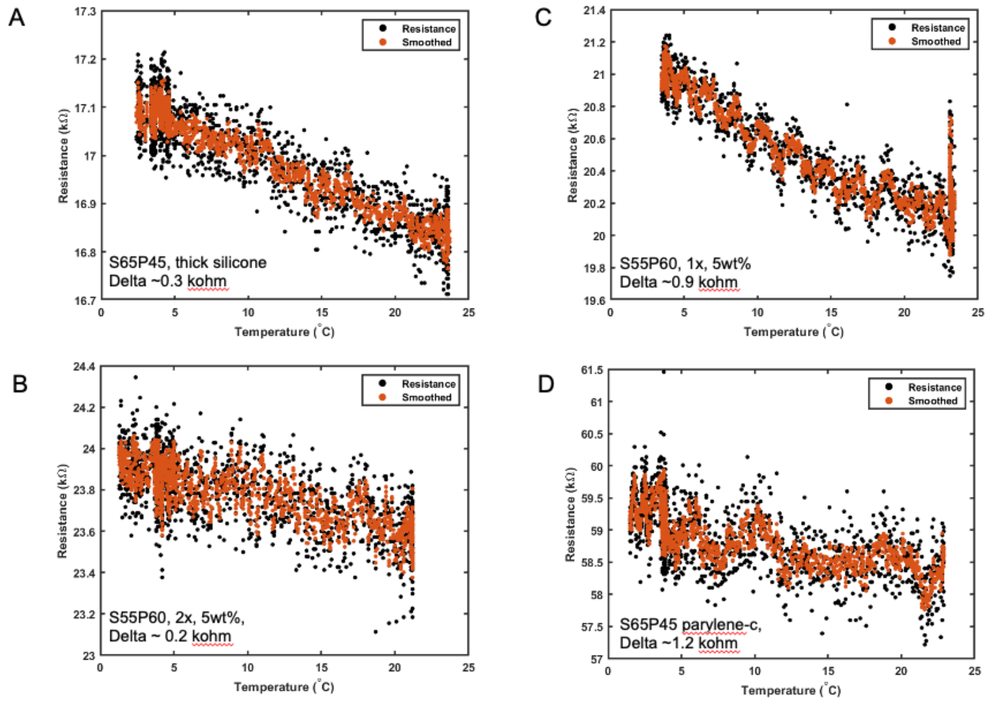

Figure 13: Change in resistance is plotted over temperature for (A) thick 10 wt% silicone layer, (B) 1x dip coat of 5 wt% silicone, (C) 2x dip coat of 5 wt% silicone, and (D) vapor deposited 1 mil parylene-c layer. Temperature range relevant to ocean depths (0 – 2 km).

Thermal and Compression Testing

To confirm that temperature was the dominant factor in resistance change over the relevant ocean temperature (0 to 25°C) and pressure ranges (0 – 1 km depth), the change in resistance with temperature was tested simultaneously with a load frame with integrated thermal chamber (MTS Systems). A Keithley source meter was used which accurately measures both applied voltage and current for direct resistance calculation. The sample was fixtured as previously described for load frame testing (no encapsulant, alligator clips), and the same load profile (0.01 in/min displacement to 1500 psi, hold 1 minute, 0.01 in/min unload to 1000 psi, hold 1 minute, unload to ~50 psi) was used. Each sample was allowed to equilibrate at different temperatures (0°C, 5°C, 15°C, and 25°C) before testing. Two successive presses were performed, and the second of each is shown in Figure 14(A). This plot confirms that there is both a thermal and pressure dependence on LIG resistance with uniaxial compression. To compare the magnitudes of change, the initial and final resistances are plotted with temperature for the same sensor, see Figure 14(B). The change in resistance with load (initial to final resistance for same temperature) is less than the change in resistance with temperature (first and last points on initial and final resistance curves). This confirms that in any fielded system integrated temperature compensation is essential, and the influence of both temperature and resistance must be characterized together.

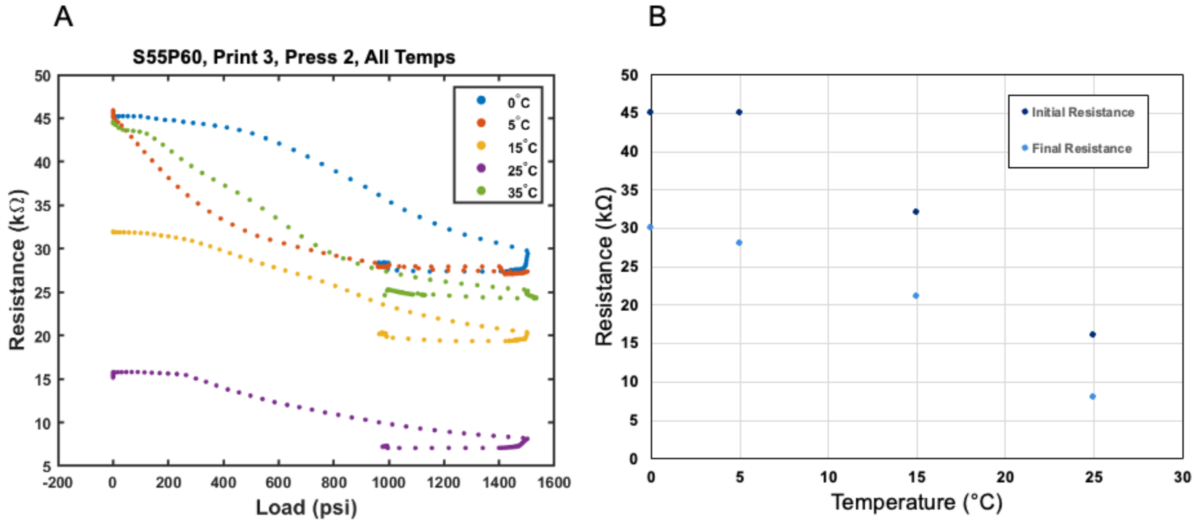

Figure 14: (A) Resistance as a function of load for different temperatures. (B) Initial and final resistances recorded for the sensor at different temperatures.

Hydrostatic Tank Testing

Finally, we characterized resistance response when pressure is applied from all directions via hydrostatic tank testing. To constrain the LIG sensor geometry, and reduce the effect of tank turbulence on pressure, sensors were constrained within acrylic holders, see Figure 15 (left.) For this measurement setup, we again attached bare wires of the LIG sensors to a PCB that was also soldered to one end of a SubConn 6 pin connector and dip coated in two layers of 10 wt% silicone. The sensors and frames were then zip tied to the wire basket and lowered into the 76-gallon hydrostatic pressure tank Figure 15 (middle). The Keithley source meter was again used to supply a current through the resistive sensor, and measure the voltage across it. The pressure was applied in 250 psi intervals up to 1500 psi, with a three-minute equilibration at each pressure. The same pressure increments and wait times were applied to the unloading cycle as well. Three different sensors were tested, one with silicone encapsulation and two with parylene-C encapsulation. Unfortunately, no distinct pressure trends were obtained. The noise of the signal was consistently higher than the resistance response during repeated tests over several days. Though resistance drop responses have been reported for similar sensors during hydrostatic tank testing in literature, we were not able to replicate these results.

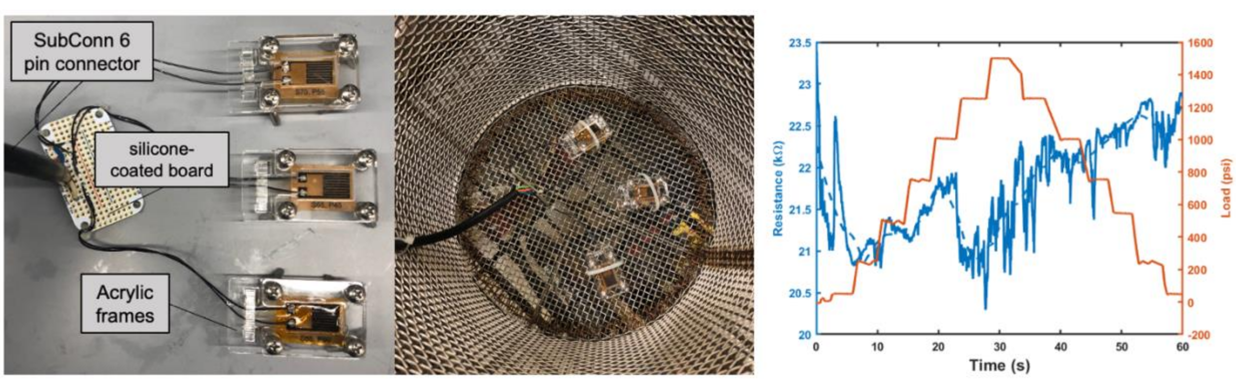

Figure 15: Hydrostatic tank testing (Left, Middle) Sensors in acrylic holders and attached to the tank. (Right) Example load profile and recorded sensor resistance.

Platform (3): Commercially Available Pressure Sensors

During the course of this project, parallel commercial advances in small form-factor and low power pressure sensors were achieved. Based on the unpredictability of custom LIG or TPU/CNT pressure sensors, we purchased a commercially available pressure sensor (Omega PX190 Rugged IP67 Compact Pressure Transmitter.) While the pressure range is lower than needed for ultimate deployment, we viewed it as a useful exercise in prototype integration and validation of hydrostatic tank testing protocol. With BlackSky electronics, we tested the response under hydrostatic pressure. The COTS sensor was soldered to the electronics board and held in place with a custom 3D printed frame while waterproof marine urethane (Scotchcast 2131) was used to pot the electronics. For tank testing, a NI DAQ logger measured the voltage change over time. Pressure was referenced to the tank internal pressure sensors and a RBR depth logger (RBRsolo[3] D). Additionally, the electronic board communicated with a custom Python script to print the output voltage internally calculated. A summary of this test, and the associated setup is shown in Figure 16 (left).

For the test, pressure was increased or decreased in 50 psi intervals from 0 psi to 250 psi to 0 psi again. The sensor was allowed to equilibrate for three minutes at each pressure, and this cycle was repeated three times. Based on these results, the pressure sensor voltage response and the processed pressure sensor voltage show good alignment with the internal tank pressure data (Figure 16, Right).

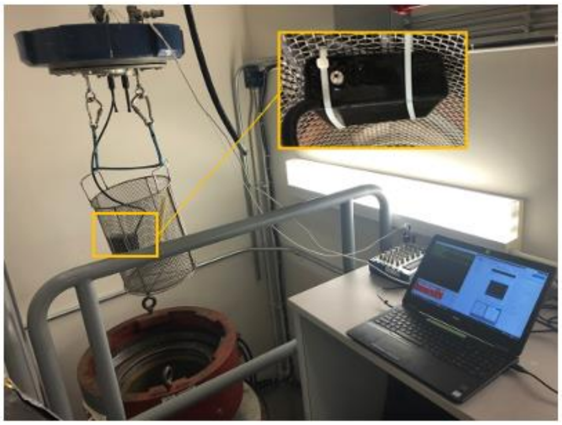

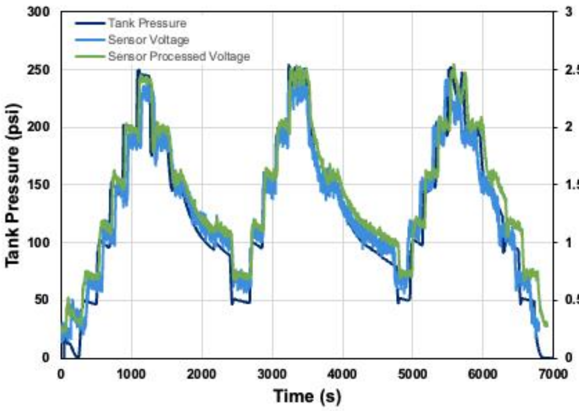

Figure 16: (Left) Hydrostatic testing of COTS pressure sensor (Omega PX190 Rugged IP67 Compact Pressure Transmitter). (Right) Example load profile and recorded sensor resistance.

B. Objective 2: Novel soft materials with antifouling properties

Summary: In this effort, we have developed and characterized novel antifouling coatings designed specifically to interface with organic materials.

Background: The adsorption of biomolecules and organisms to surfaces, known as biofouling, is a critical challenge that plagues watercraft, medical devices, and maritime sensors. In high-precision applications, such as marine sensing, biofouling can disable or even destroy expensive equipment. As oceanic monitoring becomes more crucial with the advance of climate change, it will be critical to ensure sensor accuracy, in part through biofouling prevention.

Development and Characterization of Novel Zwitterionic Anti-fouling Coatings

We have developed a two-pronged approach to combat marine biofouling: first by applying a foulant release coating (FRC) and then by irreversibly treating the surface of that coating with anti-fouling poly(zwitterions) (PZIs). We discuss the synthetic chemistry and characterization of these coatings below.

Coating systems that fully prevent the adherence of biomolecules and organisms typically operate by creating and maintaining a stable water layer between the surface of interest and the external environment. Thus, the coatings must be highly hydrophilic to swell fully and support a stable water layer. Furthermore, the coating should be charge-neutral, as biomolecules with a net charge will still be strongly coordinated to a stable water layer with a net charge. Given these restrictions, two candidates have emerged to prevent biofouling at surface through the formation of a stable water layer: poly(ethylene oxide) and PZIs.

In our approach, we initially coated a sample with a soft, physically cross-linked poly(dimethyl siloxane)-urea (PDMS-U), which is known to release biological fouling under flow generated by water current (i.e., an FRC). This release mechanism occurs due to the low hardness of the coating: under even mild strain, biological foulants will delaminate and release, clearing the surface. Then, we treat the surface with PZIs using a recently developed technique that leverages the highly reactive nitrene group. Here, a zwitterion-functionalized methacrylate is copolymerized with a proto-nitrene, i.e., a perfluoro azido benzyl methacrylate. The resulting polymer can be dissolved in saltwater and, when exposed to even mild UV light, degrade into the nitrene species and irreversibly bind the surface of interest. The synthetic approach to two-step, dual functional antifouling coatings is shown below in Figure 17.

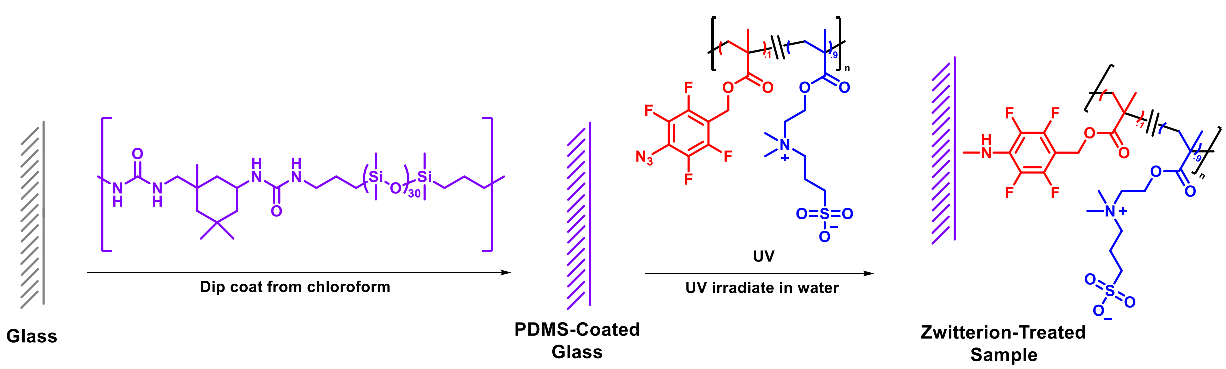

Figure 17: Synthetic approach to two-step, dual functional antifouling coatings.

PDMS-U was generated by the copolymerization of PDMS di-amine, isophorone diisocyanate, and dodecane diamine, while formation was monitored by ^{1}H NMR. The resulting material was soft, but did not flow at room temperature due to the strong hydrogen bonding of the urea groups acting as physical crosslinks. The material did flow at elevated temperatures, and was readily dissolved in dichloromethane

(DCM) and chloroform. PDMS-U was dissolved in chloroform at various weight percent and used to dip-coat glass slides. A 1 wt% solution was found to be ideal for dip coating, and yielded surfaces that were fully coated in a thin PDMS film.

PZI materials capable of treating organic surfaces were generated through the copolymerization of sulfobetaine methacrylate (commercial reagent) and a custom perfluoroazido benzyl methacrylate (PFABMA). The PFABMA was synthesized by the displacement of the *para* fluorine present in the commercial perfluoro benzyl methacrylate with sodium azide in dimethyl formamide at 70°C over three hours. The purified monomer was then copolymerized with sulfobetaine methacrylate in trifluoroethanol (TFE) using Azobisisobutyronitrile AIBN as a thermal initiator. Residual TFE was removed by rotary evaporation, and the polymer residue was re-dissolved in 0.1 M NaCl at 5 mg/mL for further use.

PDMS coated glass slides were covered with PZI solution and exposed with a variety of UV sources including a UV oven, solar radiation, and a UV wand. Effective surface treatment was measured by contact angle using a goniometer, where decreasing contact angle was indicative of a successful treatment. Over the course of 10 minutes, both the UV oven and solar radiation dramatically increased hydrophilicity. Ultimately, the UV oven treatment method was selected for further study due to the control it afforded over sample preparation.

To assess efficacy of our antifouling coating, we performed three different functional tests.

Test 1, Drip reactor with controlled microorganisms: Coated glass slides, blank glass, PDMS-U coated slides, and PDMS-U with PZI slides were loaded into a 4-channel drip reactor. Sulfitobacter was swabbed at the top of the plate, and fresh media was dripped over the samples over the course of 3 days. Samples were characterized visually for biofouling and stained with Congo Red to identify the presence of bacterial growth. Blank glass showed substantial bacterial accumulation, while PDMS-U showed some bacterial growth. Finally, the PZI samples on the whole showed less growth, but had some bacterial growth around the edges of the sample, suggesting the PDMS-U coating may be partially delaminated. Photographs are shown in Figure 18 (A).

Test 2, Marine tank with mixed community: Three aluminum panels were partially treated with our antifouling coating: the top half of the panel was left bare, the bottom half of the panel was coated with PDMS, and the bottom quarter of the panel has an additional PZI layer. Panels were exposed to running water from a marine tank with a mixed community for a total of 5 days. While results are varied, the middle sample appears as expected: the top half has the most fouling, the bottom half has less fouling, with the bottom quarter showing the least amount of fouling overall, see Figure 18 (B).

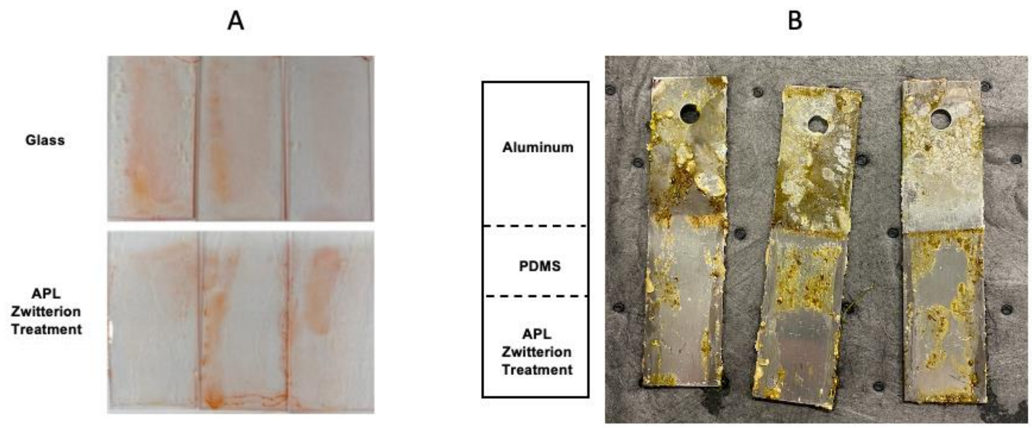

Figure 18. (A) Samples after being exposed to plating of Sulfitobacter in a drip reactor for 72 hours. Samples are stained with Congo Red for visibility. (B) Samples after being exposed to flowing water from a tank with a mixed marine community for 5 days.

Test 3, Cheasapeake Bay deployment: An aluminum panel was coated in conventional water-resistant epoxy. Half of the epoxy surface was treated with our antifouling coating, while the other half was not. These samples were then submerged in the Cheasapeake Bay at the Smithsonian Environmental Research Center (SERC) for two weeks before removal. While both sides of the panel fouled, the side treated with coating was different, suggesting modification of the fouling, while not totally reducing the fouling, Figure 19.

Figure 19. Aluminum panel coated in epoxy after 2-week exposure in the marine environment of SERC. The left side of this panel has been treated with a PZI UV treatment. While not well captured in the photo, fouling was different on the left hand side, compared to the right, indicating that the coating had some influence on biofouling.

In summary, we have developed dual-functional anti-biofouling coatings, leveraging both foulant release and novel nitrene-containing PZIs. This system can be applied to any organic coating containing a C-H bond, and can be applied under a variety of conditions including direct sunlight. While additional optimization and characterization is needed, this coating has the potential to be an impactful addition to deployed marine sensors.

C. Objective 3: System level design

Summary: The goal of this part of the work was to design low power electronics that could eventually enable a self-contained sensor platform that does not require a power or data tether. The team designed custom low power electronics for data logging and communication.

Working with APL, Blacksky Aerospace LLC designed, built, tested and evaluated electronics for low power and long-endurance operations, specifically incorporating power storage, sensor interface and sensor data readout, microcontroller-based data aggregation and storage, and data communication via an Iridium satellite modem to a control center.

Low Power and Pressure Tolerant Electronics for Long-Endurance Operation: Blacksky Aerospace LLC developed low power electronics with low quiescent current buck converters, low-power and sleep mode functionality for long-term operation and long-term shelf storage. Blacksky Aerospace LLC designed and evaluated wireless radio frequency (RF) charging electronics to enable charging an internal battery prior to system deployment or during long-term shelf storage. Relevant electronic components were designed, tested, and evaluated for pressure tolerant operation with a target of 1-1000m water depth. The use of pressure-tolerant electronics (PTE) eliminates expensive high-pressure interfaces, leading to significant cost and weight reductions.

Sensor Interface and Data Acquisition: Blacksky Aerospace LLC developed dedicated high-precision electronics to interface and readout temperature and pressure sensors. Sensor readout was adjustable within 1-30Hz. A non-volatile, ruggedized memory allowed storage of sensor data. A CPU capable of low-power and sleep mode operation was programmed to control all peripheral electronic components.

Long Range Datalink, Satellite Communication, GPS Receiver, Data Compression: While not incorporated into the final prototype, Blacksky Aerospace LLC developed dedicated long-range data communication electronics for near real-time monitoring, leveraging a bi-directional Iridium satellite modem. This capability was demonstrated in the ONR/NOPP Velella Sensor project, which ran concurrently to the Cost Effective CTD Sensor program.

The Blacksky Aerospace LLC board, including power and sensor interface/data acquisition electronics were successfully employed in the final hydrostatic pressure test with the commercial piezoelectric sensors, discussed in the previous section, reaching pressures of 250 psi.

III. Summary and Next Steps

The goal of this project was to develop a low-cost, soft-material sensor platform for oceanic salinity, temperature, and pressure (CTD) sensing. Throughout this project, we executed against the following objectives *(1): Novel sensor development*, *(2)*: *Novel soft materials with antifouling properties*, *(3)*: *System level design and prototype development*. In summary:

- We demonstrated two platforms for novel sensor development, including a TPU/CNT nanocomposite sensor, and a flexible LIG pressure sensor. We optimized and characterized the two platforms. While both showed potential, more work is needed to realize reproducible performance in the field.
- We developed a novel two-part antifouling coating, and tested the efficacy in multiple environments. This coating also shows promise, and with optimization of the coating protocol and additional characterization, this could be an impactful tool for increasing the longevity of marine sensors.
- We developed electronics for low power and long-endurance operations, which could be beneficial for multiple marine sensors, including CTD sensors and surface salinity sensors.

With additional development, we believe that technology developed within this program could contribute to the next generation of marine sensors.

IV. Dissemination to Communities of Interest?

Preliminary data of the novel salinity sensor was presented in the IEEE Oceans conference paper “Robust Ocean Salinity Sensing” in September 2021.

Long distance communication technologies and near ocean surface effects for low SWaP sensor platforms are currently being discussed with ONR and NPS.

A manuscript discussing the fabrication and characterization of laser-induced graphene pressure sensors for applications as ocean sensors is in preparation.

A manuscript discussing the TPU-CNT based pressure sensors was published in Sensors (2022).

V. Technology Transfer

JHU/APL filed a non-provisional patent application for the novel “two clock” salinity sensor in January 2022, entitled “Parallel Clock Salinity Sensor.”

VI. Participants

JHU/APL:
Leslie Hamilton
Daniel Ayoub
Joel Sarapas
Nick Kantack
Collin McDermmot
Kyle Lowery
Craig Leese
Chistine Chung
Mairead Bartlette
Brooke Luisi
Tanner Hamann
Zachary Kiick
Khamphone Inboune
Elizabeth Robinson
Zach Post
Tim Montalbano
Elizabeth Toycroft
Scott Huler
Tessa Van Volkenburg
Paul Wescoat
Christian Williams
Morgana Trexler
Amand Green
Amy Halligan

Blacksky:
Raymond Hoheisel
Sean Fox

Naval Postgraduate School (NPS):
James MacMahan

Johns Hopkins University (JHU):
Adebayo Eisape
Sung Hoon Kang

VII. Students

Tessa Van Volkenburg (APL) pursued her Doctorate of Engineering (D. Eng) with Johns Hopkins University during this time period.

Adebayo Eisape (JHU) was working towards his Ph.D. during this time.

VIII. Products

1. Conference Paper
    a. Title: Robust Ocean Salinity Sensing
    b. Authors: Kantack, Nicholas; Langevin, Spencer; Tessa, VanVolkenburg; Skerrit, Jennifer; Xia, Zhiyong; Hoheisel, Raymond; MacMahan, James; Brown, Sean
    c. Conference Name: OCEANS 2021
    d. Conference Date: 20-23 September 2021
    e. Conference Location: San Diego, USA
    f. Publication Status: Published
    g. Publication Date: 15 February 2022cdscwwdeddeedc
    h. Publication Identifier Type: DOI
    i. Publication Identifier: 10.23919/OCEANS44145.2021.9705686
    j. Acknowledgement of Federal Support? Yes

    https://ieeexplore.ieee.org/abstract/document/9705686/authors#authors

2. Patent:
    a. Patent Title: High Pressure Laser Induced Graphene Piezoresistive Pressure Sensors
    b. Patent Abstract

        Laser-induced graphene (LIG) is a porous graphene that is formed by irradiating a polyimide film with a commercial carbon dioxide laser. The laser beam breaks carbon and oxygen and carbon and nitrogen bonds at the surface, and the released gasses from this process form LIG's characteristic pores. We have used this process to pattern serpentine resistive traces on flexible polyimide films to create a piezoresistive pressure sensor, or a sensor whose resistance changes with applied load, for deep ocean pressure testing. Though this has been previously demonstrated in literature, we have found that by increasing the laser fluence, or energy per surface area, we are able to get fibrous surface morphologies that increase the sensitivity of this sensor at high pressures. We have characterized the performance of these sensors with uniaxial compression testing and hydrostatic water tank testing up to 1500 psi, or approximately 1 km of ocean depth.
    c. Patent Number 6707-2673
    d. Country of Application USA
    e. Application Date January 20, 2022
    f. Date Issued N/A
    g. Patent Application Status: submitted

3. Conference Presentation
    a. Title: Tailoring Laser-Induced Graphene Porosity for Deep Ocean Pressure Sensing
    b. Authors: Tessa Van Volkenburg, Zhiyong Xia
    c. Conference Name Materials Research Society (MRS)
    d. Conference Date November 29th – December 12nd, 2021
    e. Conference Location: The city and country where conference was held Boston, MA and virtual
    f. Publication Status (choice of: published, awaiting publication, accepted, under review, submitted, or other) published
    g. Publication Date December 7th, 2021
    h. Publication Identifier Type: n/a
    i. Publication Identifier: n/a

4. Publication
    a. Title: Soft CNT-Polymer Composites for High Pressure Sensors

b. Authors: Eisape, Adeboya; Rennoll, Valeria; Van Volkenburg, Tessa; Xia, Zhiyong; West, James; Kang, Sung Hoon
c. Journal name: sensors
d. Publication Date: 14 July 2022
e. Publication Status: Published
f. Publication Identifier Type: DOI
g. Publication Identifier: 10.33390/s22145268
h. Acknowledgement of Federal Support? Yes

https://www.mdpi.com/1424-8220/22/14/5268